

The Comparison of Cavitation Resistance of Laser Metal Deposited Layers

Abstract: Cavitation erosion is a specific case of wear, primarily affecting elements exposed to a watery environment, e.g. elements of pumps, valves and compression-ignition engines. Nickel-based alloys are regarded as materials of potentially high cavitation erosion resistance. The study discussed in the article involved the examination of cavitation erosion resistance of hardfacing layers made of NiCrBSi and NiCrBSi + 35 % wt. WC, deposited using the PPTAW method. Resistance to cavitation erosion was tested in accordance with the ASTM G-32 standard. The test results were subsequently compared with those obtained in relation to layers made of powders, the composition of which corresponded to stainless steel X5CrNiMo17-12-2 (used as a reference material). The results revealed that both nickel-based materials were characterised by significantly higher erosion resistance than that of the reference steel. The mean depth of the reference erosion of overlay welds made using X5CrNiMo17-12-2 amounted to 28.72 μm , whereas the depth of erosion in the hardfacing layers made of NiCrBSi and NiCrBSi + 35 % wt. WC amounted to 7.19 μm and 6.92 μm respectively. The above-presented differences resulted from the significantly higher hardness and plastic strain resistance of the nickel-based overlay welds than those of the steel overlay weld. It was also observed that, in spite of their higher hardness, the layers made of NiCrBSi + 35 % wt. WC were characterised by lower cavitation erosion resistance than the layers made of NiCrBSi (which could be ascribed to the chipping of the hardening phase).

Key words: plasma hardfacing, powders, metallic and cermet layers, cavitation erosion resistance

1. Introduction

Cavitation erosion is a specific case of wear, resulting from the formation of gas pores in the event of a local drop in liquid pressure and their subsequent implosion [1]. Elements exposed to this type of wear include, among other things, water turbines, marine screw propellers or fixtures used in the chemical and petrochemical industries [2]. Resistance to cavitation erosion is usually correlated with material hardness [3, 4] but also with other mechanical properties [5, 6] as well as with structure or grain size [7, 8]. The proper adjustment of surface layer (SL) properties significantly improves the operational properties of structural elements (e.g. wear resistance).

One of the methods enabling the modification of the surface layer aimed at its extended service life is hardfacing, i.e. the making of a surface layer using a material different from that of the substrate and, while doing so, applying welding technologies [9]. The most commonly used hardfacing-related welding methods include gas metal arc welding (GMAW), manual metal arc welding (MMAW) and flux-cored arc welding (FCAW) [10–12]. However, methods enjoying growing popularity are characterised by high energy concentration, e.g. laser or plasma hardfacing. In comparison with the previously enumerated welding-based hardfacing methods, laser and plasma hardfacing is characterised by higher efficiency and lower dilution [13].

In terms of hardfacing involving the use of powder plasma transferred arc welding (PPTAW), heat needed for

melting the filler metal and partly melting the base material is generated by plasma arc, generated through the mechanical constraint (narrowing) of electric arc [14]. The above-named method is commonly used in industry both in the fabrication and refurbishment of damaged machinery elements. Industrial sectors where PPTAW-based hardfacing layers are particularly commonly used include the excavation, petrochemical, metallurgical and maritime industries [13–17]. In turn, materials most commonly used as coatings include cermets [18].

Some of the most common materials used in the fabrication of hydraulic elements are stainless austenitic steels, owing their popularity to high corrosion resistance in an aqueous environment and high resistance to cavitation erosion [13, 14]. However, the above-named steels are also characterised by relatively low abrasive wear resistance, necessitating a search for solutions remedying the aforesaid disadvantage [21]. One of such solutions includes the use of nickel-based alloys, such as NiCrBSi, characterised by high corrosion resistance and wear resistance, additionally improvable by using tungsten carbide additions (WC) [22–24]. The cavitation erosion resistance of NiCrBSi alloys is described, among other things, in publications [8, 25, 26]. The objective of the study discussed in this article was the assessment of cavitation erosion resistance of nickel-based overlay welds (e.g. NiCrBSi and NiCrBSi+35% WC) as well as steel-based overlay welds (e.g. X5CrNiMo17-12-2) made using the PPTAW method.

mgr inż. Karolina Płatek, dr hab. inż. Leszek Łatka, mgr inż. Monika Górnik – Politechnika Wrocławska, Wydział Mechaniczny, Katedra Obróbki Plastycznej, Spawalnictwa i Metrologii / Wrocław University of Technology, Faculty of Mechanical Engineering, Chair of Plastic Processing, Welding and Metrology

mgr inż. Bernard Wyględacz, dr hab. inż. Artur Czupryński – Politechnika Śląska, Wydział Mechaniczny Technologiczny, Katedra Spawalnictwa / Silesian University of Technology, Faculty of Mechanical Engineering, Department of Welding

dr inż. Miroslaw Szala – Politechnika Lubelska, Wydział Mechaniczny, Katedra Inżynierii Materiałowej / Lublin University of Technology, Faculty of Mechanical Engineering, Department of Materials Engineering

Corresponding Author: leszek.latka@pwr.edu.pl

2. Test materials and methods

The materials used in the making of deposited layers were commercially available powders NiCrBSi and NiCrB-Si containing a 35% (wt.) addition of FTC-type WC (fused tungsten carbide). The tests also involved the deposition of layers made of steel X5CrNiMo17-12-2, treated as the reference material. The chemical compositions and designations of the filler metals used in the remainder of the article are presented in Table 1. The substrate was a 10 mm thick plate made of structural steel S235JR, the chemical composition of which (consistent with standard [27]) is presented in Table 2.

The powders presented in Table 1 were subjected to microscopic examination (SEM), aimed to identify their morphology. The observations were performed using a Tescan VEGA 3 microscope and secondary electron contrast. The grain-size analysis was performed using an Anton Paar PSA 1190 particle size analyser.

The hardfacing process was performed using a EuTronic Gap 3511 DC Synergic system (Castolin Eutectic, Gliwice, Poland). The identification of layer deposition parameters required the performance of hardfacing tests involving the making of single runs followed by measurements and observations aimed to selected a set of parameters for each material separately. The assessment was concerned with the presence of welding imperfections (if any), dilution and hardness. The values of variable parameters along with corresponding specimen numbers are presented in Table 3. The average value of voltage amounted to 45 V. The shielding gas was the mixture of argon with a 5% addition of hydrogen (R1-ArH-5, in accordance with standard [28]); the shielding gas flow rate was 10 l/min. The plasma gas used in the process was high-purity Argon 5.0 [28]; the gas flow rate amounted to 2 l/min. The same gas was used as powder-carrying gas (carrier gas); the gas flow rate being 3 l/min. The powder feed rates depended on the properties of the filler metals (A, B and C) and amounted to 8.98 g/min 11.15 g/min and 9.68 g/min respectively.

The specimens were subjected to visual tests (by the unaided eye), macroscopic observations, dilution-related measurements and hardness tests. The visual tests were performed directly after hardfacing. The macroscopic observations, involving cross-sectional specimens previously subjected to etching, were performed using a Keyence VHX6000 optical microscope. The specimens were etched in a 3% solution of hydrochloric and nitric acids (3:1). The visual and macroscopic tests aimed to detect welding imperfections (if any). The dilution (D) of the base material in the overlay weld material was identified in accordance with the diagram presented in Figure 1.

Vickers microhardness tests (Sinowon Innovation Metrology), involving a load of 0.98 N (HV0.1), were performed in accordance with standard [29]. The measurements were performed as presented in Figure 2.

Table 1. Chemical compositions and designations of filler metals

Designation	Powder type	Commercial name	Producer
A	NiCrBSi	Durmat 456	Durum Wear Protection GMBH, Willich, Germany
B	NiCrBSi + 35 wt. % WC	Durmat 349	Durum Wear Protection GMBH, Willich, Germany
C	X5CrNiMo17-12-2	EuTroLoy 16316	Castolin Eutectic, Gliwice, Poland

Table 2. Chemical composition of steel S235JR [wt. %] in accordance with standard [27]

C	Mn	P	S	Cu	N	Fe
0.17	1.4	0.0355	0.035	0.55	0.012	Balance

Table 3. Variable hardfacing parameters used in relation to all the powders used in the tests

	Current, I			
	80 A	100 A	120 A	
Rate, v	1.6 mm/s	Specimen 1	Specimen 4	Specimen 7
	1.2 mm/s	Specimen 2	Specimen 5	Specimen 8
	0.8 mm/s	Specimen 3	Specimen 6	Specimen 9

$$D = \frac{A_2}{A_1 + A_2}$$

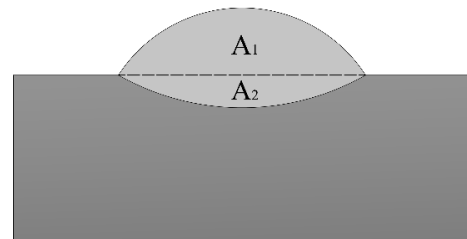


Fig. 1. Determination of dilution

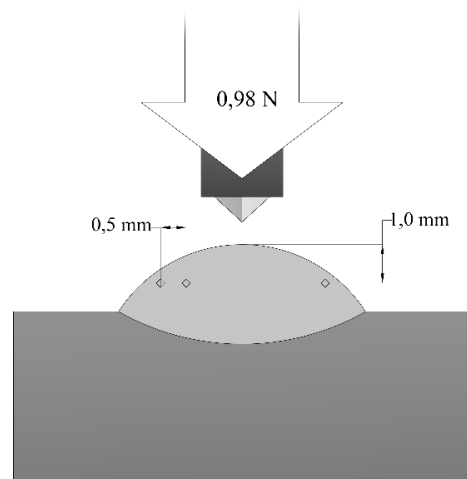


Fig. 2. Microhardness measurements

The subsequent stage involved the determination of parameters to be used when making deposited layers. The criteria governing the adjustment of parameters included the lack of welding imperfections, preferably low dilution and as high the hardness of overlay welds as possible. The

width of the layers amounted to 80 mm, whereas their length was 100 mm. Plates made of steel S235JR (100 mm × 160 mm × 10 mm) were used as the substrate. Prior to hardfacing, the plate surface was subjected to grinding and, directly before making runs, cleaned using ethanol. The value of voltage, filler metal powder feed rate, gas mixtures and gas flow rates remained unchanged in relation to conditions accompanying the making of runs. The overlap (of individual runs), dependent on the width of a single run and identified during previous tests, amounted to 30 % of the run width in terms of material B and to 40 % of the run width as regards the remaining materials (A and C). The hardfacing process was performed maintaining a constant interpass temperature of 100 °C.

The measurements of layer hardness required surface preparation performed using a magnetic grinding machine. Hardness was determined using the Vickers hardness test and a maximum load of 9.81 N. The performance of cavitation erosion resistance tests was preceded by the cutting of specimens (22 mm × 22 mm) using a CNC PROFI 300S router carving machine. Cavitation erosion resistance was tested in accordance with the ASTM G-32 standard [30]. The sonotrode diameter amounted to 15.9 mm. The frequency and amplitude of sonotrode vibration amounted to 20 kHz and 50 μm respectively. The distance between the specimen surface and the sonotrode amounted to 0.5 mm ± 0.05 mm. The working liquid was distilled water having a temperature of 25 ± 2 °C. The total time of exposure to cavitation amounted to 6 hours. The schematic diagram of the testing equipment is presented in Figure 3.

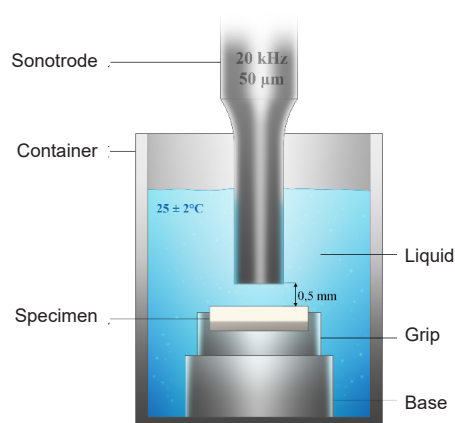


Fig. 3. Cavitation erosion resistance test

The resistance of the deposited layers to cavitation erosion was described by determining curves of mean depth erosion (MDE) and those of mean depth of penetration rate (MDPR). The mean depth of erosion is expressed as a mass decrement referred to material density and an area affected by cavitation (equal to the sonotrode diameter), whereas the maximum erosion rate indicates the largest change in the volumetric decrement of the material in time.

After the cavitation erosion resistance tests, the specimens were subjected to microscopic observations (SEM).

Table 4. Results of powder grain-size analysis

Material	d_{10} [μm]	d_{50} [μm]	d_{90} [μm]	Mean value [μm]
A	59.61 ± 0.28	82.59 ± 1.56	117.98 ± 2.13	89.07 ± 1.43
B	54.32 ± 0.44	73.07 ± 0.93	99.57 ± 1.38	78.25 ± 0.88
C	68,31 ± 0,67	96,13 ± 2,61	136,03 ± 7,38	102,79 ± 3,52

The profile of specimen roughness was measured using a Dektak 150 profile measurement gauge (Veeco Instruments Inc., Plainview, NY, USA) and a 0.8 mm Gaussian filter.

3. Test results and analysis

The morphology of the powders used in the tests is presented in microscopic photographs (SEM) (see Fig. 4). The results of granulometric measurements are presented in Table 4. In all cases, powder particles were characterised by the regular and spheroidal shape and similar sizes. However, tungsten carbide particles present in material B were different as (because of the fabrication process (crushed carbide)) they were characterised by irregular shapes and varying, sometimes significantly, sizes. In cases of spheroidal particles of metallic powders, it was also possible to notice particles of significantly smaller diameters “clung” to the surface of larger particles (see Fig. 4).

The macroscopic observations of the single-run overlay welds revealed the presence of welding imperfections (incomplete fusion) in most of the overlay welds obtained using a current of 80 A, which was particularly visible in relation to material B (Fig. 5). In addition, clearly visible wider runs were obtained in relation to the lower value of hardfacing rate. The average run width was restricted within the range of 5.86 mm (overlay weld B-1) to 14.24 mm (overlay weld B-6).

All the overlay welds were characterised by relatively high dilution (Table 5). The lowest dilution amounted to 12% (specimens C-3 and C-2), whereas the highest value of dilution amounted to 46% (specimens B-4 and B-6). The relatively high value of dilution was not favourable and could be ascribed to the powder feed method, i.e. parallel to arc. In the above-presented configuration, arc rested directly on the base material, which led to greater penetration depth and, consequently, increased dilution [11]. Regardless of the material, the lowest degree of dilution was observed in the overlay welds made using the parameters of set no. 2.

The results of hardness measurements are presented in Figure 6. As expected, the highest hardness was characteristic of the layers obtained using the composite material (overlay B) and amounted to between 496 HV0.1 ± 55 HV0.1 (specimen B-1) and 737 HV0.1 ± 131 HV0.1 (specimen B-3). The hardness of material A did not exceed 517 HV0.1 ± 69 HV0.1 (overlay weld A-1). The above-named value was similar to that presented in publications concerning coatings made of powders NiCrBSi [8, 31]. The hardness of the layers made of material C was significantly lower and amounted to 208 ± 19 HV0.1, which also corresponded to the expected hardness of coatings made of steel Cr-Ni [32].

The results of metallographic tests and hardness measurements of the single-run overlay welds were used to identify hardfacing parameters applied in the making of layers using material A (set 4), material B (set 2) and material C

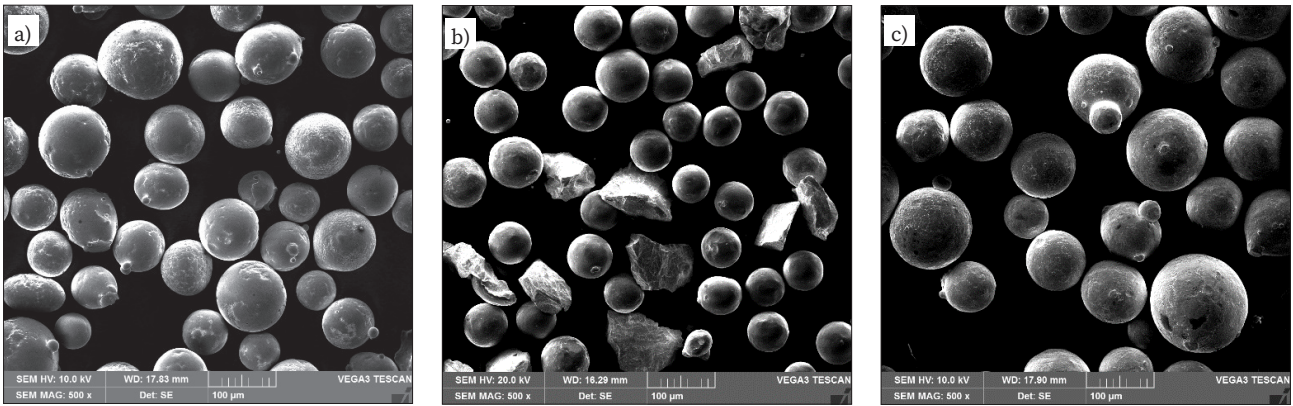


Fig. 4. Photographs (SEM) of metallic powders: a) material A, b) material B and c) material C; mag. 500×, contrast SE

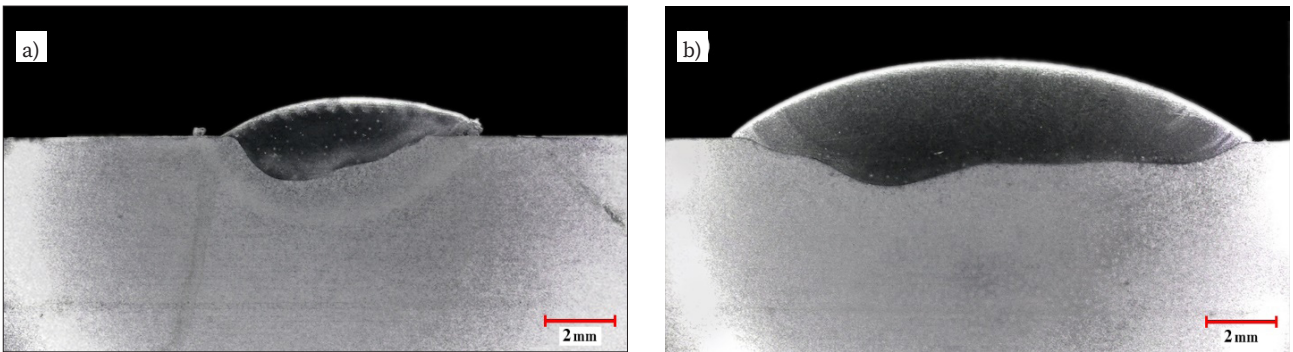


Fig. 5. Macroscopic photographs of single runs: a) overlay weld B-1, improper geometry and b) overlay weld B-3, proper geometry

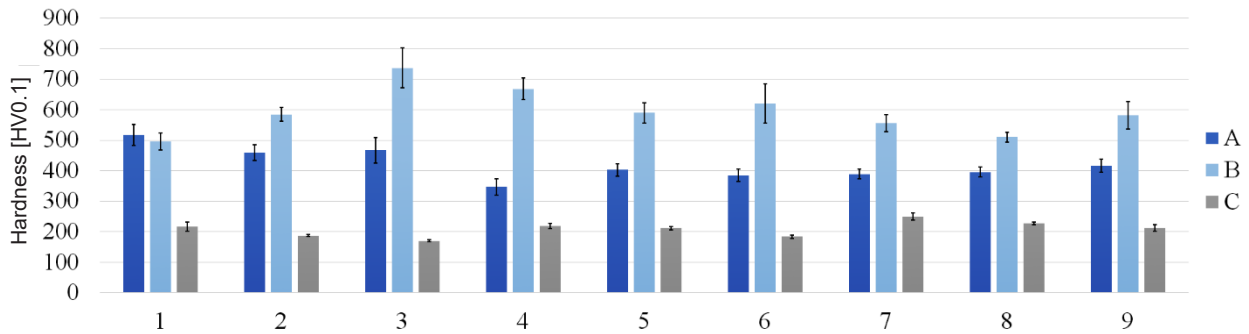


Fig. 6. Hardness measurement results obtained in relation to overlay welds A, B and C

Table 5. Dilution [%]

	1	2	3	4	5	6	7	8	9
A	42	26	13	26	45	22	32	43	31
B	28	8	26	46	21	46	44	38	41
C	21	12	12	39	40	26	40	33	28

(set 5). The exact values of variable parameters of the above-named sets are presented in Table 6.

The microstructures of the hardfacing layers are presented in Fig 7. In terms of material A it was possible to identify hard phase precipitates (carbides, carboborides and

Table 6. Parameters selected in the making of hardfacing layers

Material	Parameter set no.	Current I [A]	Hardfacing rate v [mm/s]
A	4	80	0.8
B	2	100	1.6
C	5	100	0.8

borides) deposited in the nickel-based matrix. In comparison with that of coating A, the microstructure of material B was additionally reinforced with particles of tungsten carbide (WC). The structure of overlay welds A and B corresponded to phase constituents identified in nickel-based matrixes described in publications [33, 34]. The structure of overlay weld C was dendritic, i.e. typical of hardfacing layers made of, e.g. steel Cr-Ni.

The results of cavitation tests, presented in Fig. 8, confirmed the greater reference erosion depth of steel overlay weld C in comparison with that of nickel-based overlay welds A and B, clearly indicating the lower cavitation erosion resistance of the former. After 6 hours following

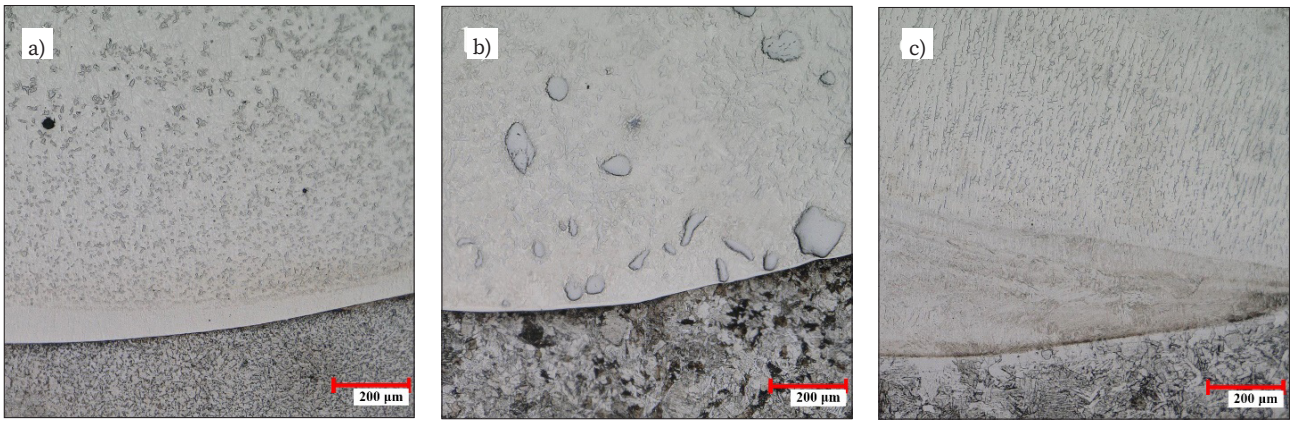


Fig. 7. Microstructure of the layers in the fusion line area: a) material A, b) material B and c) material C; etched specimens, mag. 200×

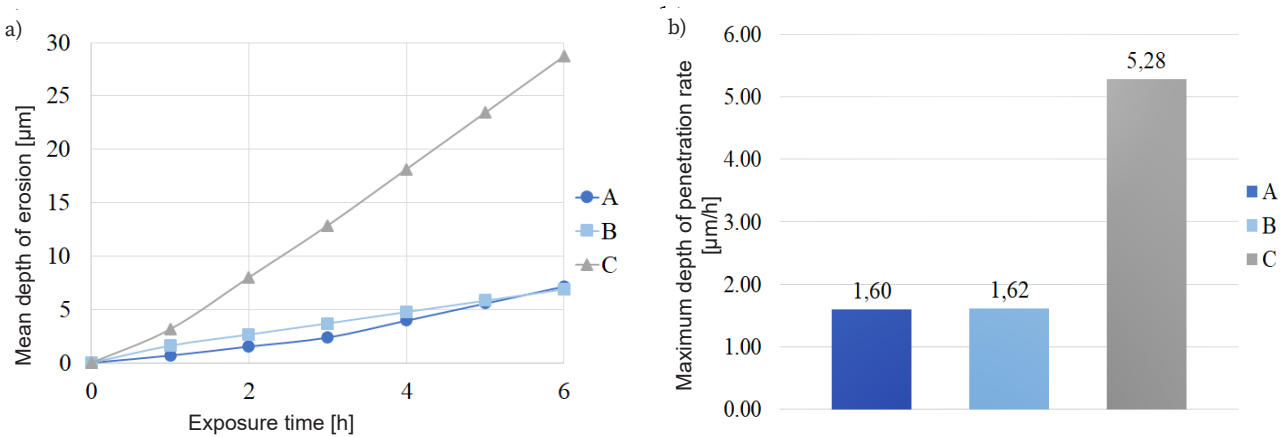


Fig. 8. Results of cavitation erosion resistance tests: a) mean depth of erosion, [μm], b) maximum depth of penetration rate, [μm/h]

the start of the test, the value of erosion depth in relation to material C amounted to 28.72 μm and was nearly four-fold higher than that observed in material A (7.19 μm) and material B (6.92 μm).

Layer C was characterised by nearly three-fold higher maximum depth of penetration rate (5.28 μm/h) than that of overlay welds A and B (1.60 μm/h and 1.62 μm/h respectively), characterised by higher erosion resistance.

The photographs (SEM) of eroded surfaces are presented in Fig. 9. The erosion of nickel-based coatings was initiated on the boundary of the nickel matrix and hard phase precipitates, leading to the formation of cracks and the removal of the material. The cavitation pits present on the

surface of material A were smaller than those identified in overlay weld B. In addition, the SEM-based surface analysis revealed that the cavitation load triggered the chipping of tungsten carbide particles from the matrix, which could additionally translate into the higher value of wear in comparison with that of the carbide-free nickel layer. The surface of material C was characterised by significant irregularities and numerous cavitation pits. The eroded surface also contained plastically deformed areas, where the removal of material was of fatigue nature.

The roughness values measured in the area w eroded surfaces (parameters Ra and Rz) are presented in Fig. 10. As expected, the greatest roughness was observed in the

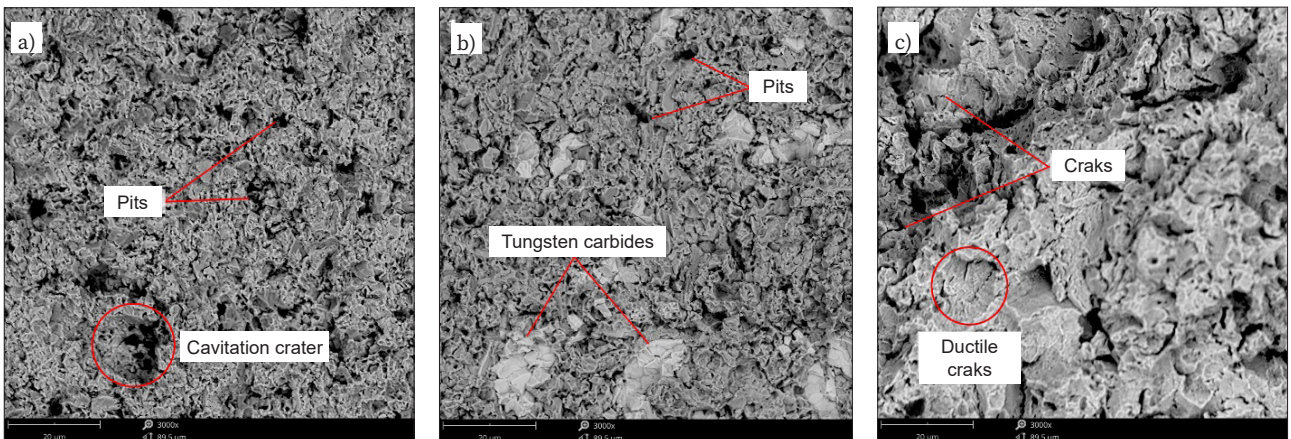


Fig. 9. Microscopic observations (SEM) of the surfaces subjected to cavitation erosion resistance tests: a) overlay weld A, b) overlay weld B and c) overlay weld C

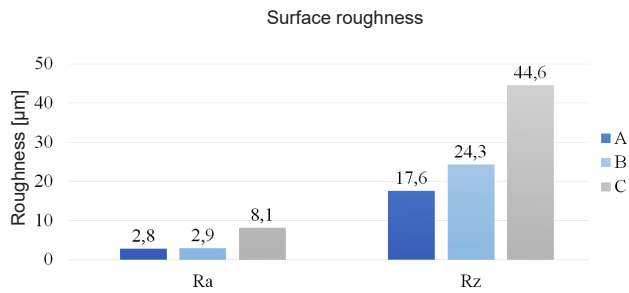


Fig. 10. Eroded roughness parameters after 6 hours of cavitation tests

material of the eroded area of specimen C, whereas the smallest was noticed in material A (characterised by the smallest loss). The values of roughness parameters R_a and R_z correlated with those of cavitation wear. Similar results were obtained in publication [8] in relation to steel AISI 304, deposited coatings NiCrBSi and cast iron. It should be emphasized that the highest roughness (designated using parameter R_a) was obtained in reference overlay weld C, whereas the values of parameters R_a and R_z related to coatings A and B were comparable.

4. Concluding remarks

The test results justified the formulation of the following conclusions:

- Both overlay weld A (NiCrBSi) and cermet overlay weld B (NiCrBSi/WC) were characterised by significantly higher cavitation erosion resistance than that of the reference overlay weld made of stainless austenitic steel. The mean depth erosion of overlay welds A, B and C amounted to 7.19 μm , 6.92 μm and 28.72 μm respectively.
- The depth of erosion pits observed on the surface of the steel reference overlay weld was significantly higher than that of the nickel-based overlay welds. Values R_a and R_z of eroded overlay weld C were nearly three-fold higher than those of overlay weld A. In relation materials A, B and C, value R_a of the test overlay welds amounted to 2.8 μm , 2.9 μm and 8.1 μm , whereas value R_z amounted to 17.6 μm , 24.3 μm and 44.6 μm for respectively.
- Overlay weld A was characterised by the lower loss of material and lower average roughness than those of overlay B, which could be ascribed to the chipping of reinforcing phase particles. The removal of tungsten carbide (WC) from overlay weld B was responsible for a significant increase in the roughness of the eroded layer.
- Overlay welds A and B were characterised by significantly higher hardness (i.e. 420 HV0.1 \pm 41 HV0.1 and 594 HV0.1 \pm 54 HV0.1 respectively) than that of layer C, the average value of which amounted to 208 HV0.1 \pm 19 HV0.1. The high hardness of the nickel-based overlay welds and their plastic strain resistance were factors favouring resistance to cavitation erosion.

REFERENCES

- [1] Steller J., Krella A.: Ocena odporności kawatycznej materiałów metodą frakcyjną. *Problemy Eksploatacji*, 2006, vol. 1, pp. 209-225.

- [2] Krella A., Zakrzewska D.: Cavitation erosion – phenomena and test rigs. *Advances in Material Science*, 2018, vol. 18, no. 2, pp. 15-27.
- [3] Heymann F.: *Erosion by Cavitation or Impingement*, ASTM, 1967.
- [4] Krella A.: Degradation and Protection of Materials from Cavitation Erosion: A Review. *Materials*, 2023, vol. 16, no. 5, no. art. 2058.
- [5] Mann B., Arya V.: An experimental study to correlate water jet impingement erosion resistance and properties of metallic materials and coatings. *Wear*, 2002, vol. 253, pp. 650-661.
- [6] Hammit F.: *Cavitation and multiphase flow phenomena*, McGraw-Hill International Book Co., New York 1980.
- [7] Zakrzewska D., Krella A.: Cavitation erosion resistance influence of material properties. *Advances in Material Science*, 2019, vol. 19, no. 4, pp. 18-34.
- [8] Szala M., Walczak M., Hejwowski T.: Factors Influencing Cavitation Erosion of NiCrSiB Hardfacings Deposited by Oxy-Acetylene Powder Welding on Grey Cast Iron. *Advances in Science and Technology Research Journal*, 2021, vol. 15, no. 4, pp. 376-386.
- [9] Klimpel A.: Industrial surfacing and hardfacing technology, fundamentals and applications, *Welding Technology Review*, 2019, vol. 91, no. 12, pp. 33-42.
- [10] Findik F.: Laser cladding and applications. *Sustainable Engineering and Innovation*, 2023, vol. 5, no. 1, pp. 1-14.
- [11] Cardoso A., Assunção E., Pires I.: Study of a hardfacing flux-cored wire for arc directed energy deposition applications. *International Journal of Advanced Manufacturing Technology*, 2022, vol. 118, no. 9-10.
- [12] Szala M., Hejwowski T.: Cavitation erosion resistance of high-alloyed Fe-based weld hardfacings deposited via SMAW method. *Tribologia*, 2022, vol. 302, no. 4, pp. 85-94.
- [13] Łatka L., Biskup P.: Development in PTA Surface Modifications – A Review. *Advances in Materials Science*, 2020, vol. 20, no. 2.
- [14] Górka J., Czupryński A., Kik T., Melcer M.: Przemysłowe aplikacje napawania plazmowego proszkowego. *Przegląd Spawalnictwa* 2011, vol. 83, no. 9, pp. 87-94.
- [15] Klimpel A., Janicki D., Lisiecki A., Wilk Z., Burda M., Klimpel A.St.: Plasma welding repair procedure for turbine jet apparatus rings in aircraft engines. *Welding International*, 2014, vol. 28, no. 6.
- [16] Kik T., Górka J., Czupryński A., Martyniszyn A.: Napawanie krawędzi przedmiotów metodami TIG i PTA. *Przegląd Spawalnictwa*, 2011, vol. 83, no. 9, pp. 79-86.
- [17] Smoleńska H., Kończewicz W., Łabanowski J.: Regeneracja zaworów silników okrętowych metodą napawania plazmowego. *Przegląd Spawalnictwa*, 2011, vol. 9, pp. 73-78.
- [18] Czupryński A., Kik T., Melcer M.: Porównanie odporności na zużycie ściernie płyt trudnościeralnych. *Przegląd Spawalnictwa*, 2018, vol. 90, no. 5, pp. 28-37.
- [19] Zakrzewska D., Buszko M., Marchewicz A., Krella A.: Concept of cavitation erosion assessment of austenitic 1.4301 stainless steel based on roughness development. *Tribology International*, 2023, vol. 183.
- [20] Ding H., Tang Q., Zhu Y., Zhang C., Yang H.: Cavitation erosion resistance of 316L stainless steel fabricated using selective laser melting. *Friction*, 2021, vol. 9, pp. 1580-1598.
- [21] Szala M., Łatka L., Walczak M., Winnicki M.: Comparative Study on the Cavitation Erosion and Sliding Wear of Cold-Sprayed Al/Al₂O₃ and Cu/Al₂O₃ Coatings and Stainless Steel, Aluminium Alloy, Copper and Brass. *Metals*, 2020, vol. 10, no. 7.
- [22] Rachidi R., El Kihel B., Delaunois F.: Microstructure and mechanical characterization of NiCrBSi alloy and NiCrBSi-WC composite coatings produced by flame spraying. *Materials Science and Engineering: B*, 2019, vol. 241, no. 2, pp. 13-21.
- [23] Guo H., Li B., Lu C., Zhou Q., Jia J.: Effect of WC-Co content on the microstructure and properties of NiCrBSi composite coatings fabricated by supersonic plasma spraying. *Journal of Alloys and Compounds*, 2019, vol. 789, no. 2, pp. 966-975.
- [24] Guo C., Zhou J., Chen J., Zhao J., Yu Y., Zhou H.: High temperature wear resistance of laser cladding NiCrBSi and NiCrB-

- Si/WC-Ni composite coatings. *Wear*, 2011, vol. 270, no. 7-8, pp. 492-498.
- [25] Daroonparvar M., Ciubotariu C.-R., Frunzaverde D., Marginean G.: Investigations of Cavitation Erosion and Corrosion Behavior of Flame-Sprayed NiCrBSi/WC-12Co Composite Coatings. *Materials*, 2022, vol. 15, no. 2943.
- [26] Zhang H.F., Zhang C.H., Wang Z.Y., Cui X., Zhang S., Chen H.T.: Microstructure and corrosion behaviour of WC/NiCrBSi coatings by vacuum cladding. *Materials Science and Technology*, 2022, no. 1, pp. 19-29.
- [27] EN 10025-european standards for structural steel, 2019.
- [28] PN-EN ISO 14175: Materiały dodatkowe do spawania – Gazy i mieszaniny gazów do spawania i procesów pokrewnych, 2009.
- [29] ISO 6507-1 – Metallic materials – Vickers hardness test – Part 1: Test method, 2005.
- [30] ASTM G32-16: Standard Test Method for Cavitation Erosion Using Vibratory Apparatus, ASTM, 2021.
- [31] Appiah A.N.S., Bialas O., Żuk M., Czupryński A., Konadu D., Adamiak M.: Hardfacing of mild steel with wear-resistant Ni-based powders containing tungsten carbide particles using powder plasma transferred arc welding technology. *Materials Science – Poland*, 2022, vol. 40, no. 3, pp. 42-63.
- [32] Prass G.S., d'Oliveira A.S.: Processing and characterization of AISI 316L coatings modified with Cu and CuO nanoparticles. *Surface and Coatings Technology*, 2023, vol. 461.
- [33] Zhou Y., Zhang J., Xing Z., Wang H., Lv Z.: Microstructure and properties of NiCrBSi coating by plasma cladding on gray cast iron. *Surface and Coatings Technology*, 2019, vol. 361, pp. 270-279.
- [34] Fernandes F., Polcar T., Loureiro A., Cavaleiro A.: Effect of the substrate dilution on the room and high temperature tribological behaviour of Ni-based coatings deposited by PTA on grey cast iron. *Surface and Coatings Technology*, 2015, vol. 281, pp. 11-19.
- [35] Hussain P., Mahmoud H., Basha S., Mohamad M.A.: Correlation between microstructure and micro-hardness of 316L nitrided austenitic stainless steel. *IOP Conference Series: Materials Science and Engineering*, vol. 863, 2020.